Inorg. Chem. **2005**, *44*, 49–60

Synthesis, Structural Characterization, and Computational Study of the Strong Oxidant Salt $[XeOTeF_5][Sb(OTeF_5)_6]\cdot SO_2ClF$†

Hélène P. A. Mercier,‡ Matthew D. Moran,‡ Jeremy C. P. Sanders,‡ Gary J. Schrobilgen,*,‡ and R. J. Suontamo§

Department of Chemistry, McMaster University, Hamilton, Ontario L8S 4M1, Canada, and Department of Chemistry, University of Jyväskylä, P.O. Box 35, FIN-40014 Jyväskylä, Finland

Received July 19, 2004

The strong oxidant salt $[XeOTeF_5][Sb(OTeF_5)_6]\cdot SO_2ClF$ has been synthesized by reaction of stoichiometric amounts of $Xe(OTeF_5)_2$ and $Sb(OTeF_5)_3$ in SO_2ClF solution at −78 °C and characterized in SO_2ClF solution by low-temperature ^{17}O, ^{19}F, ^{121}Sb, ^{125}Te, and ^{129}Xe NMR spectroscopy, showing the Xe···O donor-acceptor bond $XeOTeF_5^+\cdot SO_2ClF$ adduct-cation to be labile at temperatures as low as −80 °C. The salt crystallizes from SO_2ClF as $[XeOTeF_5][Sb(OTeF_5)_6]\cdot SO_2ClF$, and the low-temperature crystal structure was obtained: triclinic, $P\bar{1}$, $a = 9.7665(5)$ Å, $b = 9.9799(4)$ Å, $c = 18.5088(7)$ Å, $\alpha = 89.293(2)°$, $\beta = 82.726(2)°$, $\gamma = 87.433(3)°$, $V = 1787.67(13)$ Å^3, $Z = 2$, and $R_1 = 0.0.0451$ at −173 °C. Unlike MF_6^- in $[XeF][MF_6]$ (e.g., M = As, Sb, Bi) and $[XeOTeF_5][AsF_6]$, the $Sb(OTeF_5)_6^-$ anion is significantly less basic and does not interact with the coordinately unsaturated xenon(II) cation. Rather, the $XeOTeF_5^+$ cation and weak Lewis base, SO_2ClF, interact by coordination of an oxygen atom of SO_2ClF to xenon [Xe···O, 2.471(5) Å]. The $XeOTeF_5^+\cdot SO_2ClF$ adduct-cation has also been studied by low-temperature Raman spectroscopy, providing frequencies that have been assigned to adducted SO_2ClF. The solid-state Raman spectra of $XeOTeF_5^+\cdot SO_2ClF$ and $Sb(OTeF_5)_6^-$ have been assigned with the aid of electronic structure calculations. In addition to optimized geometries and vibrational frequencies, theoretical data, including gas-phase donor–acceptor bond energies, natural bond orbital (NBO) analyses, and topological analyses based on electron localization functions (ELF), provide descriptions of the bonding in $XeOTeF_5^+\cdot SO_2ClF$ and related systems. The quantum mechanical calculations provided consistent trends for the relative strengths of the Xe···O donor–acceptor bond in $XeOTeF_5^+\cdot SO_2ClF$ and ion-pair bonds in $[XeL][MF_6]$ (L = F, $OTeF_5$; M = As, Sb), with the Xe···O bond of $XeOTeF_5^+\cdot SO_2ClF$ being the weakest in the series.

Introduction

The pentafluoroorthotellurate group, $OTeF_5$, is comparable to fluorine in its ability to stabilize a variety of noble-gas species.[1,2] Derivatives of the $OTeF_5$ group are known for the 2+, 4+, and 6+ oxidation states of xenon,[3−10] as well as for the 2+ oxidation state of krypton.[11] The $OTeF_5$ analogue of the well-known XeF^+ cation, $XeOTeF_5^+$, was first obtained as the AsF_6^- salt by reaction of $FXeOTeF_5$ with AsF_5.[5] The $[XeOTeF_5][Sb_2F_{11}]$ salt was subsequently synthesized from $[XeOTeF_5][AsF_6]$ by AsF_5 displacement in liquid SbF_5.[8] The $XeOTeF_5^+$ cation has been characterized by ^{19}F, ^{125}Te, and ^{129}Xe NMR spectroscopy in SbF_5 solvent[10] and in the solid state by Raman spectroscopy of $[XeOTeF_5][AsF_6]$[5,6,9] and $[XeOTeF_5][Sb_2F_{11}]$.[10] The X-ray

* To whom correspondence should be addressed. E-mail: schrobil@mcmaster.ca.

† This work has been presented at the (a) 39th IUPAC Congress and 86th Canadian Society for Chemistry Conference, E. W. R. Steacie Award Lecture presented by G. J. Schrobilgen, Ottawa, Ontario, Aug 10−15, 2003, Abstract IN.10.001(A); (b) 227th National American Chemical Society Meeting, G. K. Surya Prakash Award Symposium, Anaheim, CA, Mar 28−Apr 1, 2004, Abstract FLUO-003; and (c) International Conference on Fluorine Chemistry '04, Kyoto, Japan, May 9−11, 2004, Abstract I-1.

‡ McMaster University.

§ University of Jyväskylä.

(1) Lentz, D.; Seppelt, K. *Angew. Chem., Int. Ed. Engl.* **1978**, *17*, 355.
(2) Birchall, T.; Myers, R. D.; de Waard, H.; Schrobilgen, G. J. *Inorg. Chem.* **1982**, *21*, 1068.
(3) Sladky, F. O. *Monatsh. Chem.* **1970**, *101*, 1559.
(4) Sladky, F. O. *Monatsh. Chem.* **1970**, *101*, 1571.
(5) Sladky, F. O. *Monatsh. Chem.* **1970**, *101*, 1578.
(6) Sladky, F. O. *Angew. Chem., Int. Ed. Engl.* **1970**, *9*, 375.
(7) Lentz, D.; Seppelt, K. *Angew. Chem., Int. Ed. Engl.* **1978**, *17*, 356.
(8) Lentz, D.; Seppelt, K. *Angew. Chem., Int. Ed. Engl.* **1979**, *18*, 66.
(9) Fir, B. A.; Mercier, H. P. A.; Sanders, J. C. P.; Dixon, D. A.; Schrobilgen, G. J. *J. Fluorine Chem.* **2001**, *110*, 89.
(10) Keller, N.; Schrobilgen, G. J. *Inorg. Chem.* **1981**, *20*, 2118.
(11) Sanders, J. C. P.; Schrobilgen, G. J. *J. Chem. Soc., Chem. Commun.* **1989**, 1576.

10.1021/ic0400890 CCC: $30.25
Published on Web 12/13/2004

crystal structure of $[XeOTeF_5][AsF_6]$ has been determined and shows that the unsaturated primary coordination sphere of $XeOTeF_5^+$, like that of XeF^+, renders it a Lewis acid that interacts with the AsF_6^- anion by means of a fluorine bridge. The resulting Xe···F cation−anion distance [2.24(3) Å][9] is significantly less than the sum of the xenon and fluorine van der Waals radii (3.63 Å)[12] and similar to that in $[XeF][AsF_6]$ [2.208(3) Å][13] and $[XeOSeF_5][AsF_6]$ [2.31(4) Å].[9]

No solid-state structural data currently exist for salts of the XeF^+ or $XeOTeF_5^+$ cations in which either XeF^+ or $XeOTeF_5^+$, or any other noble-gas cation, can be regarded as "devoid" of interactions with their nearest neighbor counteranions. Likely candidates for anions that might prove to be weakly coordinating with respect to XeF^+ and $XeOTeF_5^+$ are members of the oxidatively resistant $M(OTeF_5)_6^-$ (M = As, Sb, Bi) anion series.[14] The latter anions effectively disperse a single negative charge over 30 fluorine atoms rather than over six fluorine atoms as in their MF_6^- analogues. In addition to their low basicities, the high effective group electronegativity of the $OTeF_5$ ligands and their steric requirements in these hexacoordinate anions can be expected to make the electron lone pairs of the linking oxygen atoms less accessible to attack by strong Lewis acid oxidants. The $Sb(OTeF_5)_6^-$ anion has been shown to resist attack by the strong oxidant cations $SbCl_4^+$ and $SbBr_4^+$,[15] as well as the strongly electrophilic CCl_3^+, CBr_3^+, and $C(OTeF_5)_3^+$ cations,[16] leading to the determination of the X-ray crystal structures of their $Sb(OTeF_5)_6^-$ salts.

An earlier study from this laboratory reported the generation of $[XeOTeF_5][Sb(OTeF_5)_6]$ in SO_2ClF solution in conjunction with an attempted preparation of $Sb(OTeF_5)_5$ by reaction of equimolar amounts of $Xe(OTeF_5)_2$ and $Sb(OTeF_5)_3$.[17] The potential synthetic utility of $[XeOTeF_5][Sb(OTeF_5)_6]$ for the syntheses of main-group cationic species by oxidative elimination of a ligand (e.g., a halogen atom) bonded to the main-group element has recently been demonstrated. The strong oxidant properties of $[XeOTeF_5][Sb(OTeF_5)_6]\cdot SO_2ClF$ and the weakly basic and oxidatively resistant properties of SO_2ClF solvent[18−22] have been exploited to synthesize $Sb(OTeF_5)_6^-$ salts of the CCl_3^+, CBr_3^+, and $C(OTeF_5)_3^+$ cations by oxidation of a halide ligand atom of CCl_4 or CBr_4 with $[XeOTeF_5][Sb(OTeF_5)_6]$ in SO_2ClF solvent.[16] The carbocations have been stabilized as salts of the preformed, oxidatively resistant, and weakly coordinating $Sb(OTeF_5)_6^-$ anion, thus avoiding the use of more strongly coordinating anions derived from strong Lewis acid ligand acceptors such as SbF_5. Prior to this, generation of main-group cations by use of xenon cations as oxidants has been limited to salts of the XeF^+[23,24] and $C_6F_5Xe^+$[25] cations and had focused on the oxidation of the central element rather than on oxidative elimination of a ligand atom.

The present paper details the synthesis and structural characterization of the synthetically useful, low-temperature oxidant $[XeOTeF_5][Sb(OTeF_5)_6]\cdot SO_2ClF$ and provides an example of a noble-gas salt in which the noble-gas cation is not coordinated to its counterion. Electronic structure calculations are employed to assess bonding in the title compound and to compare the relative Lewis acid strengths of the XeF^+ and $XeOTeF_5^+$ cations and the relative Lewis basicities of SO_2ClF and the MF_6^- (M = As, Sb) anions toward both cations.

Results and Discussion

Synthesis of $[XeOTeF_5][Sb(OTeF_5)_6]$. The ability of $Xe(OTeF_5)_2$ to oxidatively introduce two $OTeF_5$ groups has been previously exploited in the syntheses of $[NR_4][Sb(OTeF_5)_6]$ salts (R = CH_3 or CH_2CH_3) from $[NR_4][Sb(OTeF_5)_4]$.[14] In the present work, a similar tack has been taken to produce a fully substituted $OTeF_5$ noble-gas salt, $[XeOTeF_5][Sb(OTeF_5)_6]$. The stoichiometric reaction of $Xe(OTeF_5)_2$ and $Sb(OTeF_5)_3$ [<1% molar excess of $Xe(OTeF_5)_2$] in SO_2ClF solvent at −20 °C (eq 1) yields bright yellow to yellow-orange solutions.

$$2Xe(OTeF_5)_2 + Sb(OTeF_5)_3 \rightarrow [XeOTeF_5][Sb(OTeF_5)_6] + Xe \quad (1)$$

Unlike its fluorine analogue, $[XeF][SbF_6]$, which is insoluble in SO_2ClF at room temperature, $[XeOTeF_5][Sb(OTeF_5)_6]$ has a high solubility (>2 M) in SO_2ClF at −78 °C. The solid salt was isolated as a pale yellow solvate, $[XeOTeF_5][Sb(OTeF_5)_6]\cdot SO_2ClF$, after pumping for several hours at −78 to 0 °C. The solid is stable to pumping at 0 °C for at least 4−5 h, but decomposes above 10 °C after 4−6 h, in marked contrast to $[XeOTeF_5][AsF_6]$[5,6,9] and $[XeF][SbF_6]$,[26] which are stable at room temperature. Solutions of $[XeOTeF_5][Sb(OTeF_5)_6]$ in SO_2ClF show significant decomposition after 30 min to 1 h at −10 °C.

Solution Characterization of $[XeOTeF_5][Sb(OTeF_5)_6]$ by ^{17}O, ^{19}F, ^{121}Sb, ^{125}Te, and ^{129}Xe Spectroscopy. The ^{19}F, ^{121}Sb, ^{125}Te and ^{129}Xe NMR spectra of $[XeOTeF_5][Sb(OTeF_5)_6]$ have been recorded at −50 °C in SO_2ClF; the corresponding chemical shifts and coupling constants are provided in Table 1. The ^{17}O NMR spectrum was recorded

(12) Bondi, A. *J. Phys. Chem.* **1964**, *68*, 441.
(13) Elliott, H. S. A.; Lehmann, J. F.; Jenkins, D. H. B.; Schrobilgen, G. J., to be published.
(14) Mercier, H. P. A.; Sanders, J. C. P.; Schrobilgen, G. J. *J. Am. Chem. Soc.* **1994**, *116*, 2921.
(15) Casteel, W. J.; Kolb, P.; LeBlond, N.; Mercier, H. P. A.; Schrobilgen, G. J. *Inorg. Chem.* **1996**, *35*, 929.
(16) Mercier, H. P. A.; Moran, M. D.; Schrobilgen, G. J.; Steinberg, C.; Suontamo, R. J. *J. Am. Chem. Soc.* **2004**, *126*, 5533.
(17) Syvret, R. G.; Mitchell, K. M.; Sanders, J. C. P.; Schrobilgen, G. J. *Inorg. Chem.* **1992**, *31*, 3381.
(18) Olah, G. A.; Donovan, D. J.; Lin, H. C. *J. Am. Chem. Soc.* **1976**, *98*, 2661.
(19) Peterson, P. E.; Brockington, R.; Vidrine, D. W. *J. Am. Chem. Soc.* **1976**, *98*, 2660.
(20) Gillespie, R. J.; Riddell, F. G.; Slim, D. J. *J. Am. Chem. Soc.* **1976**, *98*, 8069.
(21) Calves, J.-Y.; Gillespie, R. J. *J. Am. Chem. Soc.* **1977**, *99*, 1788.
(22) Olah, G. A.; Donovan, D. J. *J. Am. Chem. Soc.* **1978**, *100*, 5163.
(23) Minkwitz, R.; Bäck, B. In *Inorganic Fluorine Chemistry, Toward the 21st Century*; Thrasher, J. S., Strauss, S. H., Eds.; ACS Symposium Series: American Chemical Society: Washington, DC, 1994; Vol. 555, Chapter 6, p 90.
(24) Brown, D. R.; Clegg, M. J.; Downs, A. J.; Fowler, R. C.; Minihan, A. R.; Norris, J. R.; Stein, L. *Inorg. Chem.* **1992**, *31*, 5041.
(25) Frohn, H.-J.; Klose, A.; Henkel, G. *GIT Fachz. Lab.* **1993**, *37*, 752.
(26) Selig, H.; Holloway, J. H. In *Topics in Current Chemistry*; Boschke, F. L., Ed.; Springer-Verlag: Berlin, 1984; Vol. 124, pp 33−90.

Table 1. ^{19}F, ^{125}Te, ^{129}Xe, ^{17}O, and ^{121}Sb NMR Parameters for [XeOTeF$_5$][Sb(OTeF$_5$)$_6$][a]

species	chemical shift (δ), ppm					coupling constant, Hz		
	^{19}F[b]	^{125}Te	^{129}Xe	^{17}O[c]	^{121}Sb	$^2J(^{19}F_A-^{19}F_X)$[b]	$^1J(^{19}F-^{125}Te)$[b]	$^1J(^{19}F-^{123}Te)$
XeOTeF$_5^+$	−51.7 (F_A) −40.3 (F_X)	579.9	−1459.5	133		175	3776 (F_A) 3810 (F_X)	
Sb(OTeF$_5$)$_6^-$	−42.4 ($F_A \approx F_B$)	548.4		107	−13		3553	2950

[a] All NMR spectra were recorded in SO$_2$ClF solvent at −50 °C, except for the ^{17}O spectrum, which was recorded at −15 °C. [b] The subscripts A and B/X denote axial and equatorial fluorine atoms, respectively. [c] The ^{17}O NMR parameters for solvent SO$_2$ClF at natural abundance were also determined in the present study: doublet at $\delta(^{17}O)$, 227.0 ppm; $^2J(^{17}O-^{19}F)$, 27.9 Hz.

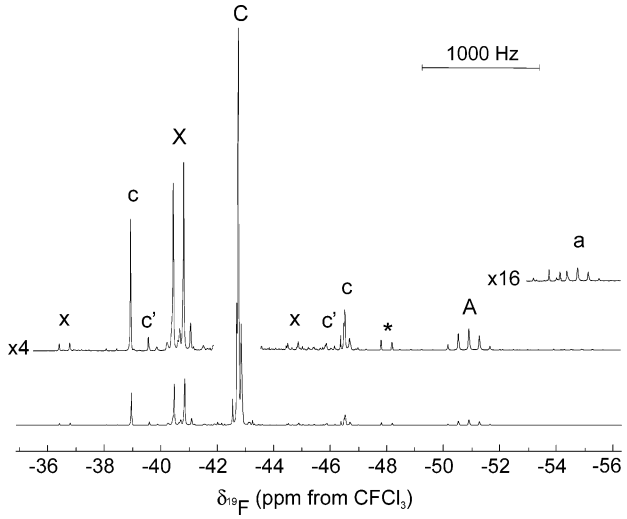

Figure 1. ^{19}F NMR spectrum (470.571 MHz) of [XeOTeF$_5$]-[Sb(OTeF$_5$)$_6$]·SO$_2$ClF in SO$_2$ClF solvent at −80 °C, where the labels A and X denote the AX$_4$ spectrum of XeOTeF$_5^+$ and C denotes the A and B$_4$ parts of the severe AB$_4$ spectrum of Sb(OTeF$_5$)$_6^-$. Peaks denoted by a, x, and c are ^{125}Te satellites that arise from $^1J(^{19}F-^{125}Te)$, and peaks denoted by c' are ^{123}Te satellites that arise from $^1J(^{19}F-^{123}Te)$. The asterisk (∗) denotes the X part of the AX$_4$ spectrum of unreacted B(OTeF$_5$)$_3$.

for an enriched [^{17,18}O]-[XeOTeF$_5$][Sb(OTeF$_5$)$_6$] sample at −15 °C, which was prepared according to eq 1 by reaction of natural-abundance Sb(OTeF$_5$)$_3$ with a stoichiometric amount of enriched [^{17,18}O]-Xe(OTeF$_5$)$_2$ (^{16}O, 35.4%; ^{17}O, 21.9%; ^{18}O, 42.7%).

The ^{19}F NMR spectrum of [XeOTeF$_5$][Sb(OTeF$_5$)$_6$] (Figure 1) consists of an AX$_4$ pattern, assigned to the XeOTeF$_5^+$ cation, that is well-resolved at 11.744 T with accompanying ^{123}Te ($I = {}^1/_2$, 0.87%) and ^{125}Te ($I = {}^1/_2$, 6.99%) satellites and a second very severe AB$_4$ pattern, with ^{123}Te and ^{125}Te satellites, that is assigned to the Sb(OTeF$_5$)$_6^-$ anion. The AB$_4$ pattern of Sb(OTeF$_5$)$_6^-$ is severely higher order, even at a field strength of 11.744 T, as a result of the near equivalence of the equatorial and axial fluorine environments, appearing as a single, intense broadened line and three weaker lines that are similar in appearance to those previously reported for the anion at the same field strength.[14] Consequently, it is neither possible to provide a value for $^2J(^{19}F_A-^{19}F_B)$ nor to differentiate the chemical shifts of F_A and F_B; however, these parameters have been estimated in a previous study.[15] The ^{19}F resonances of the anion are accompanied by ^{123}Te and ^{125}Te satellites having asymmetric line shapes that arise from the higher-order AB$_4$ portion of the AB$_4\Omega$ ($\Omega = {}^{123}$Te or ^{125}Te) spin systems.[14]

The ^{125}Te NMR spectrum of XeOTeF$_5^+$ consisted of a well-resolved binomial doublet of quintets [$\delta(^{125}$Te), 579.9 ppm] arising from $^1J(^{125}Te-^{19}F_A)$ (3776 Hz) and $^1J(^{125}Te-^{19}F_X)$ (3810 Hz). The doublet of quintets of the Sb(OTeF$_5$)$_6^-$ anion is more shielded (548.4 ppm) and is broadened, appearing as a pseudo-sextet [$^1J(^{125}Te-^{19}F_{A,B})$, 3550 Hz]. The line broadening is a consequence of quadrupolar relaxation by the antimony nuclides (^{121}Sb, $I = {}^5/_2$, 57.25%; ^{123}Sb, $I = {}^7/_2$, 42.75%) that results in near-complete collapse of the $^2J(^{125}Te-^{121,123}Sb)$ couplings.

The ^{129}Xe NMR spectrum consists of a singlet at −1489.0 ppm ($\Delta\nu_{1/2}$ = 388 Hz) in the xenon(II) region of the spectrum. In contrast to the previously reported low-field (2.1139 T) NMR study of this cation in SbF$_5$ solvent at 25 °C [$\delta(^{129}$Xe), −1472 ppm; $^3J(^{129}Xe-^{19}F_X)$, 18.5 Hz],[10] the $^3J(^{129}Xe-^{19}F_X)$ coupling was not resolved, and is a consequence of the increased relaxation rate and line width that attend the higher field strength used to record the spectrum in the present study. The increased relaxation rate is attributed to shielding anisotropy, which is expected to be large in xenon(II) species,[27] and is proportional to the square of the applied field.[28]

The ^{121}Sb NMR spectrum consisted of a broad singlet at −13 ppm ($\Delta\nu_{1/2}$ = 1240 Hz), which is in good agreement with the previously reported chemical shift of the Sb(OTeF$_5$)$_6^-$ anion in CH$_3$CN solvent.[14] The large line width and inability to observe the $^2J(^{125}Te-^{121}Sb)$ coupling reported for this anion in CH$_3$CN is most likely a consequence of the higher viscosity of SO$_2$ClF and lower temperature used to record the spectrum, leading to a longer rotational correlation time and shorter relaxation time.[29]

The ^{17}O spectrum of [^{17,18}O]-[XeOTeF$_5$][Sb(OTeF$_5$)$_6$] gave two broad, partially overlapping singlets. The most intense spectral feature was at 133.3 ppm ($\Delta\nu_{1/2}$ = 1350 Hz), which is assigned to the Sb(OTeF$_5$)$_6^-$ anion. The weaker resonance at 107.0 ppm ($\Delta\nu_{1/2}$ = 980 Hz) is assigned to the XeOTeF$_5^+$ cation. The latter resonance is shifted to lower frequency with respect to those of Xe(OTeF$_5$)$_2$ (152.1 ppm) and FXeOTeF$_5$ (128.8 ppm) recorded in SO$_2$ClF solvent at −16 °C.[11] The low-frequency shift (shielding) with respect to the parent molecules upon XeOTeF$_5^+$ cation formation is analogous to that observed for XeF$^+$ and XeF$_2$.[30]

(27) Gerken, M.; Hazendonk, P.; Nieboer, J.; Schrobilgen, G. J. *J. Fluorine Chem.* **2004**, *125*, 1163.
(28) Howarth, O. W. In *Multinuclear Magnetic Resonance*; Mason, J., Ed.; Plenum Press: New York, 1987; Chapter 5.
(29) Sanders, J. C. P.; Schrobilgen, G. J. In *Proceedings of the NATO Advanced Study Institute on Methodological Approach to Multinuclear NMR in Liquids and Solids—Chemical Applications*; Granger, P., Harris, R. K., Eds.; Kluwer Academic Publishers: Dordrecht, The Netherlands, 1988; Vol. 322, pp 172−181.

Table 2. Crystallographic Data for $[XeOTeF_5][Sb(OTeF_5)_6]\cdot SO_2ClF$

chem formula	$O_9F_{36}SClSbTe_7Xe$
space group	$P\bar{1}$
a (Å)	9.7665(5)
b (Å)	9.9799(4)
c (Å)	18.5088(7)
α (deg)	89.293(2)
β (deg)	82.726(2)
γ (deg)	87.433(3)
V (Å^3)	1787.67(13)
molecules/unit cell	2
mol wt (g mol^{-1})	2041.76
calcd density (g cm^{-3})	3.793
T (°C)	−173
μ (mm^{-1})	7.656
R_1[a]	0.0451
wR_2[b]	0.0930

[a] R_1 is defined as $\sum|F_o| - |F_c|/\sum|F_o|$ for $I > 2\sigma(I)$; wR_2 is defined as $[\sum[w(F_o^2 - F_c^2)^2]/\sum w(F_o^2)^2]^{1/2}$ for $I > 2\sigma(I)$.

Although SO_2ClF is a very weak Lewis base and has been extensively used as a solvent medium for strong Lewis acid fluoride ion acceptors, ^{19}F NMR studies of MF_5 (M = As,[31] Sb[32]) in SO_2ClF and in SO_2F_2 have shown that, unlike SO_2F_2, SO_2ClF is sufficiently basic to form weak donor−acceptor adducts with strong Lewis acid pentafluorides at low temperatures. Although Raman spectroscopy and single-crystal X-ray crystallography of the $[XeOTeF_5][Sb(OTeF_5)_6]\cdot SO_2ClF$ have shown that SO_2ClF solvent is coordinated through an oxygen atom to the xenon atom of the $XeOTeF_5^+$ cation (see X-ray Crystal Structure of $[XeOTeF_5][Sb(OTeF_5)_6]\cdot SO_2ClF$ and Raman Spectroscopy), the ^{19}F NMR spectrum provides no direct evidence for coordinated SO_2ClF. This is attributed to the lability of the Xe···O donor−acceptor bond in solution that results in rapid chemical exchange between the bulk SO_2ClF solvent molecules and coordinated SO_2ClF at temperatures as low as −80 °C.

X-ray Crystal Structure of $[XeOTeF_5][Sb(OTeF_5)_6]\cdot SO_2ClF$. A summary of the refinement results and other crystallographic information is provided in Table 2. Important bond lengths and bond angles are listed in Table 3 along with the calculated values. The structure consists of well-separated $XeOTeF_5^+$ cations and $Sb(OTeF_5)_6^-$ anions in which each $XeOTeF_5^+$ cation is oxygen-coordinated to an SO_2ClF molecule (Figure 2).

The structural parameters for the $Sb(OTeF_5)_6^-$ anion are in good agreement with those previously reported for $M(OTeF_5)_6^-$ (M = As, Sb, Bi)[14−16,33] and with those calculated in this work (see Computational Results and Table S1) and therefore require no further comment.

The $XeOChF_5^+$ (Ch = Se, Te) cations have been characterized in their AsF_6^- salts, where all $XeOChF_5^+$ bond lengths and bond angles were influenced by four-fold orientational disorders.[9] The $XeOChF_5^+$ cations were, however, shown to be strongly ion-paired with their AsF_6^- anions by means of fluorine bridges, a structural feature that is also encountered in XeF^+ salts.[9,13,34] In contrast, the $XeOTeF_5^+$ cation in the current structure is neither coordinated to the anion nor disordered. Rather, the xenon atom of $XeOTeF_5^+$ is coordinated through an oxygen atom of the

Table 3. Experimental and Calculated Geometrical Parameters for the $XeOTeF_5^+\cdot SO_2ClF$ Adduct-Cation

	bond lengths (Å)			bond angles (deg)	
	exptl	calcd[a] (C_1)		exptl	calcd[a] (C_1)
Xe(1)−O(7)	1.969(4)	1.998	Xe(1)−O(7)−Te(7)	120.8(2)	117.4
Te(7)−O(7)	1.938(5)	1.958	O(7)−Te(7)−F(33)	177.2(2)	179.7
Te(7)−F(33)	1.810(4)	1.826	O(7)−Te(7)−F(31)	86.6(2)	87.4
			O(7)−Te(7)−F(32)	91.4(2)	88.9
			O(7)−Te(7)−F(34)	89.5(2)	88.8
			O(7)−Te(7)−F(35)	88.6(2)	87.4
Te(7)−F(31)	1.813(4)	1.834	F(33)−Te(7)−F(31)	90.6(2)	92.3
Te(1)−F(32)	1.831(4)	1.854	F(33)−Te(7)−F(32)	91.3(2)	91.3
Te(7)−F(34)	1.829(4)	1.855	F(33)−Te(7)−F(34)	90.9(2)	91.3
Te(7)−F(35)	1.817(4)	1.834	F(33)−Te(7)−F(35)	91.0(2)	92.4
			F(31)−Te(7)−F(32)	177.8(2)	176.1
			F(31)−Te(1)−F(34)	90.1(2)	90.7
			F(31)−Te(7)−F(35)	90.3(2)	90.6
			F(32)−Te(7)−F(34)	89.0(2)	87.7
			F(32)−Te(7)−F(35)	90.6(2)	90.8
			F(34)−Te(7)−F(35)	178.1(2)	176.0
Xe(1)···O(8)	2.479(4)	2.388	O(7)−Xe(1)···O(8)	174.2(2)	175.2
S(1)−O(9)	1.437(5)	1.423	O(9)−S(1)−O(8)	115.7(2)	119.5
S(1)−O(8)	1.429(5)	1.476	O(9)−S(1)−F(36)	109.6(3)	109.8
S(1)−F(36)	1.474(5)	1.549	O(9)−S(1)−Cl(1)	108.2(4)	114.1
S(1)−Cl(1)	1.932(2)	1.958	O(8)−S(1)−F(36)	110.6(3)	104.5
			O(8)−S(1)−Cl(1)	108.4(2)	106.8
			Cl(1)−S(1)−F(36)	103.6(2)	100.0
			Xe(1)···O(8)−S(1)	139.6(3)	122.5

[a] SVWN/SDB-cc-pVTZ.

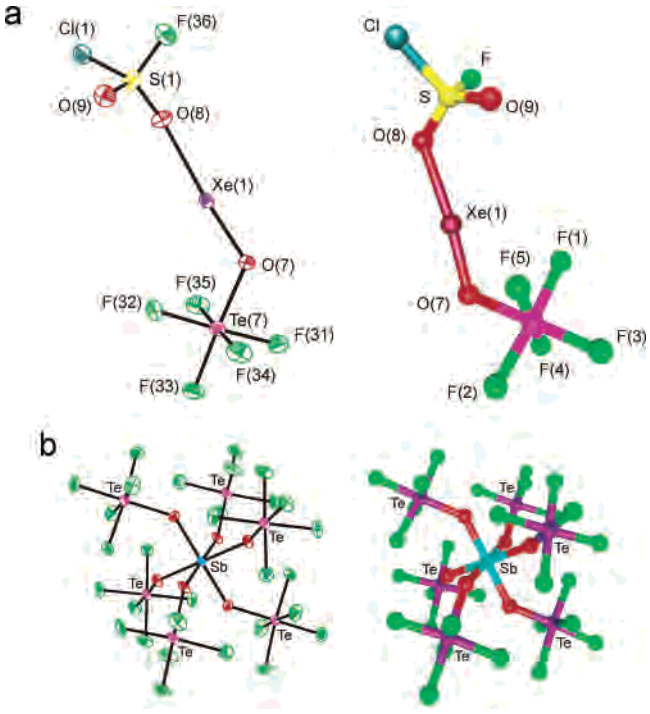

Figure 2. X-ray crystal structures of (a) $XeOTeF_5^+\cdot SO_2ClF$ and (b) $Sb(OTeF_5)_6^-$ in $[XeOTeF_5][Sb(OTeF_5)_6]\cdot SO_2ClF$; thermal ellipsoids are shown at the 50% probability level. Calculated geometries of the $XeOTeF_5^+\cdot SO_2ClF$ adduct-cation and $Sb(OTeF_5)_6^-$ anion appear on the right-hand side.

(30) Gerken, M.; Schrobilgen, G. J. *Coord. Chem. Rev.* **2000**, *197*, 335.
(31) Brownstein, M.; Gillespie, R. J. *J. Am. Chem. Soc.* **1970**, *92*, 2718.
(32) Dean, P. A. W.; Gillespie, R. J. *J. Am. Chem. Soc.* **1969**, *91*, 7260.
(33) Gerken, M.; Kolb, P.; Wegner, A.; Mercier, H. P. A.; Borrmann, H.; Dixon, D. A.; Schrobilgen, G. J. *Inorg. Chem.* **2000**, *39*, 2813.
(34) Holloway, J. H.; Hope, E. G. *Adv. Inorg. Chem.* **1998**, *46*, 51.

weak Lewis base solvent molecule SO_2ClF, forming the adduct-cation $XeOTeF_5^+\cdot SO_2ClF$. The difference in solid-state coordination behavior is attributed to the weakly coordinating nature of the $Sb(OTeF_5)_6^-$ anion relative to those of the AsF_6^-, SbF_6^-, $Sb_2F_{11}^-$, and related anions derived from strong Lewis acid pentafluorides (vide supra; also see Computational Results). The authors have recently reported the crystal structure of $[C(OTeF_5)_3][Sb(OTeF_5)_6]\cdot 3SO_2ClF$ in which two of the three SO_2ClF solvent molecules in the formula unit are oxygen-coordinated to the carbon atom along the pseudo-three-fold axis of the $C(OTeF_5)_3^+$ cation.[16] To the authors' knowledge, the only other published example of a crystal structure in which SO_2ClF forms an oxygen-coordinated adduct with a Lewis acid center is $Fe(OTeF_5)_3\cdot 3SO_2ClF$.[35]

Any comparison of the geometric parameters determined for the present structure with those of $[XeOTeF_5][AsF_6]$ is compromised by disorder in the latter structure (vide supra).[9] The absence of disorder in the present structure, however, allows valid comparisons to be made with the geometric parameters of $Xe(OTeF_5)_2$.[9] As anticipated, and by analogy with XeF^+ salt formation from XeF_2,[34] the Xe−O(7) distance [1.969(4) Å] is shorter than that in neutral $Xe(OTeF_5)_2$ [2.119(11) Å] and is consistent with the calculated increases in bond orders for Xe−F and Xe−O (also see Computational Results). The Te−O(7) bond distance [1.938(5) Å] in $XeOTeF_5^+$ is significantly longer than that in $Xe(OTeF_5)_2$ [1.843(11) Å], which is consistent with the increased bond order and decreased bond length of the Xe−O(7) bond trans to it. The Te−F bond distances of the $XeOTeF_5^+$ cation (Table 3) are similar to those found in other $OTeF_5$ compounds.[14−16,33]

When compared with those in free SO_2ClF,[36] the S−Cl and S−F bond lengths of the adducted SO_2ClF molecule are shorter, whereas the lengths of both the coordinated and uncoordinated S−O bonds in the adduct-cation have increased and are equal to within $\pm 3\sigma$. The S−O bond lengthenings and S−F and S−Cl bond contractions are corroborated by lower SO_2 and higher S−F/S−Cl vibrational stretching frequencies (see Raman Spectroscopy).

Although the Xe···O(8) distance points to a significant covalent interaction between the xenon and oxygen atoms based on a comparison of the sum of the xenon and oxygen van der Waals radii (vide supra), the S−O bond lengths of coordinated SO_2ClF are only marginally longer than those of free SO_2ClF (vide infra). The latter observation is consistent with a very weak Xe···O donor−acceptor bond, but is at apparent odds with the short Xe···O(8) distance [2.471(5) Å]. Comparison of the Xe···O(8) distance with the sums of the van der Waals radii of xenon and oxygen might not be valid because the distribution of the three equatorial valence-electron lone-pair domains of xenon that are associated with the AX_2E_3 VSEPR arrangement of the near-linear O(8)···Xe−O(7) moiety is not spherical, but toroidal in shape, allowing the incoming electron lone pair of the oxygen donor atom to approach more closely (see Computational Results). Similar contacts have been noted in the structures of $[C(OTeF_5)_3][Sb(OTeF_5)_6]\cdot 3SO_2ClF$[16] and $Fe(OTeF_5)_3\cdot 3SO_2ClF$,[35] where two and three SO_2ClF molecules, respectively, coordinate to the central atom. The S−O bonds of the coordinated SO_2ClF molecules are also equal, within $\pm 3\sigma$, to those of uncoordinated SO_2ClF, with the exception of one coordinated S−O bond in $Fe(OTeF_5)_3\cdot 3SO_2ClF$ that is significantly elongated.

A number of weak inorganic oxygen bases such as COF_2,[37,38] SOF_2,[37] SO_2F_2,[37] SO_2,[37] $PO_2F_2^-$,[39] and POF_3[37] have been studied by vibrational spectroscopy and shown to form oxygen-coordinated adducts with AsF_5 and SbF_5. The only other example of a weak inorganic oxygen base coordinated to a strong Lewis acid of which the authors are aware that has been structurally characterized by X-ray crystallography is $SbF_5\cdot SO_2$. In this instance, the terminal S−O bond [1.402(4) Å] is contracted and that of the coordinated oxygen is elongated [1.469(4) Å] relative to the S−O bond lengths of free SO_2 [1.434(1) Å].[40]

The Xe−O(7)−Te angle [120.8(2)°] is comparable to that reported previously for $Xe(OTeF_5)_2$ [122.3(5)°]. The Xe···O(8) donor−acceptor bond distance [2.471(5) Å] is longer than the Xe−O(7) bond, but is significantly shorter than the sum of the xenon and oxygen van der Waals radii (3.68 Å)[12] and has been reproduced by electronic structure calculations (see Computational Results). The O(7)−Xe···O(8) angle [174.2(2)°] deviates slightly from the anticipated linear AX_2E_3 VSEPR arrangement characteristic of Xe(II) compounds and is similar to the O−Xe···F bridge angle observed in $[XeOTeF_5][AsF_6]$ [174(1)°].[9] The O(7)−Xe···O(8) and Xe−O(7)−Te angles are reproduced by the gas-phase, energy-minimized structure, but the experimental Xe···O(8)−S angle is larger than the calculated value (Table 3). The difference is likely a consequence of crystal packing, anion−cation interactions, and the weak covalent nature of the Xe···O(8) donor−acceptor bond. The angle deformation might, in part, stem from four interionic contacts that occur around xenon [range, 3.065(4)−3.231(4) Å] that are significantly shorter than the sum of xenon and fluorine van der Waals radii (3.63 Å).[12]

Raman Spectroscopy. (a) $XeOTeF_5^+\cdot SO_2ClF$. Series of low-temperature Raman spectra were recorded for several $SO_2ClF/[XeOTeF_5][Sb(OTeF_5)_6]\cdot SO_2ClF$ ratios at −160 °C (Table S2), permitting assignments to be made of modes arising from coordinated and uncoordinated SO_2ClF based on changes in their relative intensities. The relative ratios of free SO_2ClF and coordinated SO_2ClF were determined by integration of the in-phase SO_2 stretching bands of coordinated and uncoordinated SO_2ClF in their Raman spectra. Changes in SO_2ClF composition did not result in significant relative intensity or frequency changes for the vibrational modes of either $XeOTeF_5^+$ or $Sb(OTeF_5)_6^-$. The final spectrum corresponding to $[XeOTeF_5][Sb(OTeF_5)_6]\cdot SO_2ClF$ is

(35) Drews, T.; Seppelt, K. *Z. Anorg. Allg. Chem.* **1991**, *606*, 201.
(36) Mootz, D.; Merschenz-Quack, A. *Acta Crystallogr.* **1988**, *C44*, 924.
(37) Chen, G. S.; Passmore, J. *J. Chem. Soc., Dalton Trans.* **1979**, 1257.
(38) Hoge, B.; Boatz, J. A.; Hegge, J.; Christe, K. O. *Inorg. Chem.* **1999**, *38*, 3143.
(39) Christe, K. O.; Gnann, R.; Wagner, R. I.; Wilson, W. W. *Eur. J. Solid State Inorg. Chem.* **1996**, *33*, 865.
(40) Haase, J.; Winnewisser, M. *Z. Naturforsch. A* **1968**, *23*, 61.

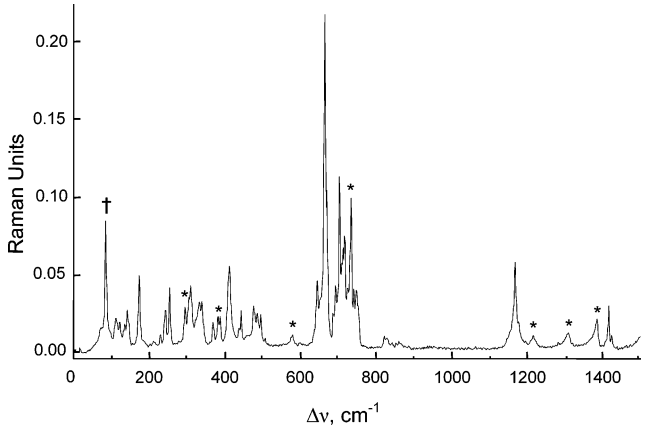

Figure 3. Raman spectrum of $[XeOTeF_5][Sb(OTeF_5)_6]\cdot SO_2ClF$ recorded at −160 °C using 1064-nm excitation; asterisks (*) and the dagger (†) denote FEP sample tube lines and an instrumental artifact, respectively.

shown in Figure 3, and the frequencies, intensities, and assignments of the vibrational bands are provided in Table 4.

The Raman assignments for the adduct-cation, $XeOTeF_5^+\cdot SO_2ClF$, were made by comparison with the calculated frequencies and were also guided by previous vibrational assignments for SO_2ClF[41] and $XeOTeF_5^+$,[5,6,9] as well as by more recent detailed assignments provided in the Supporting Information (Tables S3 and S4, respectively). Calculations of the vibrational frequencies were carried out at the HF and DFT levels of theory using Stuttgart and (SDB-)cc-PVTZ basis sets, but only the DFT results are reported in Table 4 (also see Supporting Information, Table S5). The experimental and calculated frequencies for SO_2ClF, $XeOTeF_5^+$, and $XeOTeF_5^+\cdot SO_2ClF$ and the assignments for $XeOTeF_5^+\cdot SO_2ClF$ are also provided in Table 4. The present assignments for SO_2ClF are in agreement with those reported for the neat liquid,[41] but are now more precisely described. The present assignments for $XeOTeF_5^+$ reproduce the published assignments for this cation.[9] The $XeOTeF_5^+$ cation is expected to be more weakly coordinated in the $Sb_2F_{11}^-$ salt than in $[XeOTeF_5][AsF_6]$ and thus represents a better approximation of a weakly coordinated $XeOTeF_5^+$ cation. For this reason, the vibrational frequencies of $XeOTeF_5^+$ in $[XeOTeF_5][Sb(OTeF_5)_6]\cdot SO_2ClF$ are compared with, and found to be most similar to, those of $[XeOTeF_5][Sb_2F_{11}]$[10] (Table 4).

The Raman spectrum of a sample containing a 7.95:1.00 molar ratio of SO_2ClF to $[XeOTeF_5][Sb(OTeF_5)_6]\cdot SO_2ClF$ showed several frequencies assigned to uncoordinated SO_2ClF that were slightly shifted with respect to those of pure solid SO_2ClF and liquid SO_2ClF (Tables 4 and S3). The bands that were observed at 436, 486, and 1166 cm^{-1} were assigned to coordinated SO_2ClF (vide infra).[42] At a 1.09:1.00 molar ratio, the bands associated with uncoordinated SO_2ClF greatly diminished in intensity, while the three bands assigned to coordinated SO_2ClF gained in intensity and several new, but weaker, bands appeared that are also assigned to coordinated SO_2ClF. Finally, in the Raman spectrum of a sample containing no free SO_2ClF, the bands attributed to uncoordinated SO_2ClF are absent, and the spectrum of coordinated SO_2ClF is better resolved (Table S2). The calculated vibrational frequencies show that the formation of the adduct-cation is accompanied by low-frequency shifts of the strongly coupled in-phase and out-of-phase SO_2 stretching modes, while the SF and SCl stretches are shifted to higher frequency relative to those of free SO_2ClF. Unlike free SO_2ClF, the SF stretching mode is weakly coupled to the in-phase SO_2 stretching mode. The SO_2ClF stretching modes show no significant coupling with the cation stretching modes. The TeF_5 group and out-of-phase XeOTe stretching frequencies between 645 and 735 cm^{-1} are little affected by complexation with SO_2ClF, so their mode descriptions are the same as in uncomplexed $XeOTeF_5^+$. The in-phase XeO(7)Te and bridging XeO(8) stretching modes are strongly coupled, and their in-phase and out-of-phase components, in turn, couple with the SO(8)FCl umbrella bend. Aside from four modes that are pure $XeOTeF_5^+$ (286, 296, 296 cm^{-1}) and SO_2ClF (275 cm^{-1}) modes, all modes below 316 cm^{-1} are strongly coupled deformation and torsional modes involving both $XeOTeF_5^+$ and SO_2ClF (Table 4).

There is good agreement between observed and calculated frequencies in Table 4; moreover, the observed frequency shifts arising from complexation are also reproduced. The in-phase and out-of-phase SO_2 stretching modes exhibit the anticipated low-frequency shift upon complexation, while the ν(SF) and ν(SCl) modes shift to higher frequency relative to those of free SO_2ClF. The low-frequency shifts of the strongly coupled SO_2 stretching modes and the high-frequency shifts of the sulfur−halogen stretching modes are consistent with the increased S−O bond lengths and the shorter S−F and S−Cl bond lengths observed in the crystal structure. Whereas the S−O bond order is expected to decrease for the S−O bond of the coordinated oxygen atom, the terminal S−O bond order is expected to increase, but to a lesser extent. This is supported by the NBO analyses and is accompanied by increased S−F and S−Cl bond orders. The frequency shifts and calculated bond orders are also consistent with increased negative charge on the coordinated oxygen atom and a smaller decrease in negative charge on the terminal oxygen atom (see Computational Results).

Although the S−O bond length differences in $SbF_5\cdot SO_2$ are clearly distinguishable and the terminal S−O bond is significantly shorter than the coordinated S−O bond, the strongly coupled in-phase and out-of-phase SO_2 stretching modes of this adduct are also shifted to lower frequencies when compared with those of free SO_2. Other examples of main-group oxide fluorides that function as Lewis bases (e.g., COF_2,[37,38] SOF_2,[37] SO_2F_2,[37] SO_2,[37] $PO_2F_2^-$,[39] and POF_3[37]) and form oxygen-coordinated adducts with AsF_5 and/or SbF_5 show analogous decreases in ν(CO), ν(SO), $\nu(SO_2)$, and $\nu(PO_2)$ and increases in ν(CF), ν(SF), and ν(PF) when compared with the corresponding frequencies of the free donor species.

The experimental difference between the in-phase and out-of-phase SO_2 stretching frequencies (Δ) of SO_2ClF increases

(41) Craig, N. C.; Futamura, K. *Spectrochim. Acta A* **1989**, *45*, 507.
(42) The frequency of the band at 1166 cm^{-1} is identical to that in ref 16 for coordinated SO_2ClF observed in the $CBr_{3-n}(OTeF_5)_n^+$ system.

Table 4. Experimental and Calculated Vibrational Frequencies for SO_2ClF, $XeOTeF_5^+$, and $XeOTeF_5^+ \cdot SO_2ClF$

SO_2ClF			$XeOTeF_5^+$		$XeOTeF_5^+ \cdot SO_2ClF$		
calcd[a]	liquid[b]	solid[c]	calcd[a]	$Sb_2F_{11}^-$ salt[d]	calcd[a]	exptl[e]	assgnts (C_1)[f]
1453(183)	1450(5)	1441(6) 1437(4) 1431(18)			1389(172)	1423(6) 1415(14)	$\nu(SO_2)$ o.o.p
1214(141)	1217(51)	1215(18) 1208(28) 1205(31)			1100(734)	1177(10) 1168(27) 1155(8) 1147(5)	$\nu(SO_2)$ i.p.
799(183)	820(10)	826(8) 819(30)			856(158)	860(4) 830(5)	ν(SF) + some $\nu(SO_2)$ i.p.
			746(83)	748(2)	735(75)	745, sh[g]	ν(TeF3−TeO7) + ν(TeF1−TeF2) + ν(TeF4−TeF5)
			740(82)	741(14)	730(180)	741(19)[g]	ν(TeO7−TeF3) + ν(TeF1−TeF2) + ν(TeF4−TeF5)
			739(89)		732(97)	734(49)[g]	ν(TeF1−TeF2) + ν(TeF5−TeF4)
			675(20)	714(23)	676(176)	716, sh 712(23)	ν(TeO7−XeO7) + $\nu(TeF_5)$
			659(5)	671(64)	650(8)	669(48)	ν(TeF1+TeF2) − ν(TeF4+TeF5)
			655(12)	661(31)	645(99)	663(100)	ν(XeO7−TeO7) + $\nu(TeF_{4e})$
597(199)	624(33)	612(61)			630(203)		ν(SCl) + $\delta(SFO_2)$
465(12)	502(7)	508(29)	478(30)	487(41) 474, sh	510(39) 483(13)	506(5) 493(12)	ν(XeO7+TeO7) − ν(XeO8) + δ(SO8FCl) ν(XeO7+TeO7) + ν(XeO8) − δ(SO8FCl) + some $\delta(SO_2)$
440(13)	476(6)	481(24)			453(14)	486(13) 478, sh 476(15)	$\rho_t(SO_2)$ + δ(OSF) + ν(XeO8)
393(<1)	425(100) 418(45)	431(100) 426(46)			414(6)	442(14)[h] 436(8)	ν(SCl) − $\delta(SFO_2)$
			305(90)	320(4) 311(10)	316(44)	322(11) 310(21)	ν(XeO8) − TeF_{4e} umbrella + some [δ(F4TeF1) − δ(F5TeF2)] + δ(SFCl) ± $\rho_t(SO_2)$ ± ρ_t(SFCl)
			293(22)	293(9)	304(93)	298(15)	ν(XeO8) + TeF_{4e} umbrella − some [δ(F4TeF1) − δ(F5TeF2)] + δ(SFCl) ± $\rho_t(SO_2)$ ± ρ_t(SFCl)
			290(35)		296(31) 296(31)	295(15)	δ(TeO7F3F4F5) umbrella + ρ_r(F2TeF1) δ(TeO7F3F2F1) umbrella + ρ_r(F4TeF5)
			290(7)	252(28)	286(1)	249(15)	δ(F4TeF2) + δ(F1TeF5)
279(<1)	306(16)	313(25) 310(13)			275(<1)		δ(FSCl) ± $\rho_t(SO_2)$ ± ρ_t(SFCl) + some torsions
266(<1)	294(13)	295(11)	254(3)		272(3)	254(20)	[δ(F3TeF1) + δ(F3TeF5)] + [δ(O7TeF2) + δ(O7TeF4)]
			234(2)	210(3)	234(9)		[δ(F3TeF2) + δ(F3TeF5)] − [δ(F3TeF4) + δ(F3TeF1)]
			186(<1)	173(31)	193(<1)	187(4)	ρ_t(TeF1F3F4) + ρ_t(TeF5F2O7)
			157(1)		172(35)	173(22)	δ(FSCl) + ρ_w(FSCl) + ν(XeO8) + δ(XeO7Te) + δ(F4TeF1) i.p. + ρ_w(F2TeF5) + [δ(XeO7Te) i.p. + δ(O7TeF3) i.p.]
			138(<1)	125(4)	160(<1) 132(4)	121(10)	δ(F3TeO7) + ρ_r(F4TeF1) + ρ_t(F2TeF5) $\rho_r(SO_2)$ + ρ_w(SFCl) + ρ_r(TeF5F4F3) + ρ_w(F1TeF2) in the TeF_{4e} plane + ν(XeO8)
			88(1)		109(<1) 101(5) 59(1)		strongly coupled deformation and torsion modes involving both $XeOTeF_5^+$ and SO_2ClF + lattice modes
			31(1)		49(<1) 20(0) 17(0) −5(<1)		

[a] SVWN/(SDB-)cc-pVTZ; infrared intensities, in km mol^{-1}, are given in parentheses [b] Values for liquid SO_2ClF (22 °C). [c] Values for solid SO_2ClF (−163 °C). [d] Values taken from ref 10. [e] Frequencies are from column III in Table S2. [f] The labeling scheme corresponds to that in Figure 2a (calculated, right-hand side). Bond elongation and angle opening are denoted by plus (+) signs, and bond contraction and angle closing are denoted by negative (−) signs. The symbols and abbreviations denote stretch (ν), bending (δ), twisting (ρ_t), wagging (ρ_w), rocking (ρ_r), in-plane bending (i.p.), and out-of-plane bending (o.o.p.) modes. The in-plane and out-of-plane motions of SO_2ClF are relative to the S,O(8),O(9) plane in Figure 2a whereas the in-plane motions of the $XeOTeF_5^+$ group are relative to the Xe,O(7),Te,F(3) plane in Figure 2a. [g] Both $XeOTeF_5^+$ and $Sb(OTeF_5)_6^-$ have a band that is coincident at this frequency. [h] The ν(SCl) mode of the $XeOTeF_5^+ \cdot SO_2ClF$ adduct-cation displays a $^{35}Cl/^{37}Cl$ isotope splitting (6.2 cm^{-1}), in close agreement with the previously published[42] value of 7 cm^{-1} and the values obtained in the present study (liquid SO_2ClF, 7.0 cm^{-1}; solid at −143/−163 °C, 6.8/6.7 cm^{-1}).

from 218 cm^{-1} (solid mixtures), 226 cm^{-1} (pure solid, −163 °C), and 233 cm^{-1} (pure liquid, 22 °C) in uncoordinated SO_2ClF to 246 cm^{-1} in coordinated SO_2ClF. The increase in Δ is consistent with the difference in the S−O bond orders that results from complexation and is reflected in the S−O bond orders of the bridging Xe−O−S moiety (1.14) and the terminal S−O bond (1.29) (see Computational Results). Similar increases in Δ have been observed for the $F_5M\cdots OSO$ (M = Sb, As) adducts (185 cm^{-1} in free SO_2; 225 (Sb) and 206 (As) cm^{-1} in the adduct) and for $F_5As\cdots OPF_2O\cdots AsF_5^-$ (165 cm^{-1} in $PO_2F_2^-$; 197 cm^{-1} in the complex anion).

(b) $Sb(OTeF_5)_6^-$. The prior vibrational assignments[14,43] for $Sb(OTeF_5)_6^-$ have been improved and are presented in the Supporting Information (Table S6).

Computational Results. (a) Geometry of $XeOTeF_5^+ \cdot SO_2ClF$. The electronic structure of the $XeOTeF_5^+ \cdot SO_2ClF$ adduct has been calculated starting from C_1 symmetry using

(43) Cameron, T. S.; Krossing, I.; Passmore, J. *Inorg. Chem.* **2001**, *40*, 4488.

Hartree−Fock (HF) and pure density functional theory (DFT) methods and Stuttgart and (SDB-)cc-pVTZ basis sets, yielding an optimized geometry having C_1 symmetry. Although both types of calculations resulted in stationary points with all frequencies real for SO_2ClF and $XeOTeF_5^+$, the energy minimizations of the $XeOTeF_5^+ \cdot SO_2ClF$ adduct cation gave rise to a local minimum at the HF level, but gave one imaginary frequency at the DFT level (Table 4). Overall, the DFT method gave better agreement between the experimental and calculated geometries and vibrational frequencies. For this reason, only the DFT results are reported in this paper; the other calculated values can be found in the Supporting Information (Table S5). The $XeOTeF_5^+$ cation[9,16] and SO_2ClF[16] have been the subject of previous theoretical calculations. They were, however, recalculated in the present study at the same level of theory as $XeOTeF_5^+ \cdot SO_2ClF$ in order to study the changes in geometric parameters and vibrational frequencies that occur upon coordination. The present optimized geometric parameters for SO_2ClF (C_s) and $XeOTeF_5^+$ (C_1) are listed in the Supporting Information (Tables S3 and S4, respectively).

Overall, there is very good agreement between the calculated and observed geometries, particularly for the Xe−O−Te and O−Xe···O angles. The largest deviation is for the O−S−O···Xe dihedral angle [calcd, −13.2°; obsd, 24.9(6)°], which is expected because it can be more easily deformed by crystal packing. At the HF level, the O−Xe···O bond angle is almost linear, and the Xe−O bond is shorter than the Te−O bond. The HF method has previously been shown to incorrectly predict linear geometries for the $Xe_2F_3^+$[44] and $Kr_2F_3^+$[45] cations. Although there is no crystal structure containing a well-isolated $XeOTeF_5^+$ cation, the calculated geometry of $XeOTeF_5^+ \cdot SO_2ClF$ shows several significant changes when compared with the calculated geometry of the $XeOTeF_5^+$ cation. As expected, the Xe−O bond length increases upon coordination; the F_a−Te−F_e angles are smaller, moving the equatorial fluorine atoms away from the oxygen atom, while the Te−O and Te−F bond lengths and the Xe−O−Te angle remain essentially unchanged. As observed experimentally, the calculated S−F and S−Cl bond lengths are found to be shorter than in free SO_2ClF, while the coordinated S−O(8) bond is found to be elongated and the terminal S−O(9) bond length is comparable to that in uncomplexed SO_2ClF. The calculated geometrical changes are also in accord with changes observed in the structures of the $SbF_5 \cdot SO_2$ adduct[46] and $Fe(OTeF_5)_3 \cdot 3SO_2ClF$.[35] The increase in Cl−S−F bond angle and corresponding decrease in O−S−O bond angle relative to the experimental values of uncomplexed SO_2ClF are reproduced at both levels of theory.

(b) Bonding in $XeOTeF_5^+ \cdot SO_2ClF$ and Related Systems. Natural bond orbital (NBO) and electron localization function (ELF) analyses have been performed for XeF_2; free XeF^+; the $XeOTeF_5^+ \cdot SO_2ClF$ adduct-cation; and the [XeF][SbF_6], [XeF][AsF_6], [$XeOTeF_5$][SbF_6], and [$XeOTeF_5$][AsF_6] ion pairs to (1) determine the relative strengths of the Xe···F and Xe···O donor−acceptor interactions and (2) correlate the valence-electron lone-pair basin distribution with the strength of the donor−acceptor interaction. The total xenon lone-pair basin volumes and f_{sep}-values are given in Figures 4, S1, and S2. Further details associated with the NBO and ELF analyses are provided in Tables 5, S7, and S8.

Table 5. Calculated[a] Natural Atomic Charges, Mayer Bond Orders, and Mayer Natural Atomic Orbital Valencies for SO_2ClF, $XeOTeF_5^+$, and $XeOTeF_5^+ \cdot SO_2ClF$

	$XeOTeF_5^+ \cdot SO_2ClF$	$XeOTeF_5^+$	SO_2ClF
	Charge		
Xe(1)	1.16	1.18	
O(7)	−0.95	−0.87	
Te(1)	3.52	3.51	
F(33)	−0.56	−0.55	
F(31)	−0.56	−0.55	
F(32)	−0.60	−0.59	
F(34)	−0.60	−0.59	
F(35)	−0.56	−0.55	
S(1)	2.18		2.18
O(8)	−0.87		−0.78
O(9)	−0.74		−0.78
Cl(1)	−0.003		−0.17
F(36)	−0.39		−0.44
	Valency		
Xe(1)	0.68	0.58	
O(7)	0.97	0.99	
Te(1)	3.22	3.20	
F(33)	0.52	0.53	
F(31)	0.50	0.51	
F(32)	0.48	0.49	
F(34)	0.48	0.49	
F(35)	0.50	0.51	
S(1)	3.63		3.60
O(8)	1.06		1.02
O(9)	1.06		1.02
Cl(1)	0.64		0.56
F(36)	0.55		0.52
	Bond Order		
Xe(1)−O(7)	0.47	0.54	
Te(1)−O(7)	0.55	0.49	
Te(1)−F(33)	0.55	0.56	
Te(1)−F(31)	0.54	0.54	
Te(1)−F(32)	0.51	0.52	
Te(1)−F(34)	0.51	0.52	
Te(1)−F(35)	0.54	0.54	
Xe(1)···O(8)	0.16		
S(1)−O(8)	1.03		1.15
S(1)−O(9)	1.18		1.15
S(1)−Cl(1)	0.76		0.67
S(1)−F(36)	0.66		0.62

[a] SVWN/(SDB-)cc-pVTZ.

Gas-phase complexation energies were calculated at the SVWN/(SDB-)cc-pVTZ level and were exothermic for [XeF][AsF_6]/[XeF][SbF_6] (−149.2/−145.8 kcal mol^{-1}), [$XeOTeF_5$][AsF_6]/[$XeOTeF_5$][SbF_6] (−133.3/−130.0 kcal mol^{-1}), and $XeOTeF_5^+ \cdot SO_2ClF$ (−27.8 kcal mol^{-1}), showing that the ion-pairing energies are greater for XeF^+ than for $XeOTeF_5^+$ for both AsF_6^- and SbF_6^-, and that the donor−acceptor interaction between $XeOTeF_5^+$ and SO_2ClF is only ca. 20% that of the fluorine-bridge bond energy in the AsF_6^- and SbF_6^- salts and ca. 50% of the complexation energy for $XeF^+ \cdot H_2O$ (−51.7 kcal mol^{-1}). At the opposite end of the

(44) Fir, B. A.; Gerken, M.; Pointner, B. E.; Mercier, H. P. A.; Dixon, D. A.; Schrobilgen, G. J. *J. Fluorine Chem.* **2000**, *105*, 159.
(45) Lehmann, J. F.; Dixon, D. A.; Schrobilgen, G. J. *Inorg. Chem.* **2001**, *40*, 3002.
(46) Minkwitz, R.; Molsbeck, W.; Preut, H. *Z. Naturforsch. B: Chem. Sci.* **1989**, *44*, 1581.

scale, the complexation energy for XeF^+ and naked F^- ion (-259.7 kcal mol^{-1}), leading to XeF_2 formation, is approximately twice the aforementioned ion-pairing energies.

Gas-phase thermodynamic donor−acceptor bond strengths are corroborated by the higher bond orders for Xe···F(7) in [XeF][AsF$_6$]/[XeF][SbF$_6$] (0.216/0.199) than for Xe···F(6) in [XeOTeF$_5$][AsF$_6$]/[XeOTeF$_5$][SbF$_6$] (0.197/0.192) and by the lower natural charges on xenon in [XeOTeF$_5$][AsF$_6$]/[XeOTeF$_5$][SbF$_6$] (1.194/1.195) when compared to those for xenon in [XeF][AsF$_6$]/[XeF][SbF$_6$] (1.222/1.232). Each fluorine [F(6) and F(7)] that has a long contact to the xenon atom of the ion pair, is assigned four valence-electron pairs by their NBO analyses. The longer M···F(6) and M···F(7) bridge bond lengths and their lower bond orders indicate considerably weaker, less-covalent bonding when compared with the terminal M−F bond strengths of the anions. The calculated terminal M−F bond lengths in the ion pairs are shorter and their bond orders are slightly higher and more covalent for AsF_6^- than for SbF_6^-. The interaction between F_5TeOXe^+ and SO_2ClF is shown to be considerably weaker and more ionic, having a Xe···O(3) bond order of only 0.164 and a larger charge difference on the donor and acceptor atoms [Xe, 1.159; O(3), −0.868].

When ELF isosurface contours are drawn at progressively increasing function values (*f*), the basins separate at f_{sep} and the lobes thus formed contain more localized electron density with increasing *f*-value (Figure 4). In the case of the lone-pair (monosynaptic) basins, a noteworthy feature is the toroidal valence-electron pair density on xenon and the more exposed core charge at the "openings" of the torus. The torus results from the combination of the three nonbonding ELF basins corresponding to the three electron-lone-pair domains of XeF_2 in its AX_2E_3 VSEPR arrangement of bond pair domains (X) and valence-electron lone-pair domains (E). Thus, the valence electron lone pairs are not individually localized. The three-dimensional xenon valence isosurface is similar in appearance to that of isovalent ClF_2^-.[47] All xenon(II) species considered in the present study exhibit toroidal xenon valence electron-pair basins, with XeF_2 providing the most symmetric example (Figure S1). For the AXE_3 VSEPR arrangement of XeF^+, the xenon valence lone-pair density also forms a torus; however, it is asymmetric, and the opening opposite the Xe−F bond exposing the core basin density is more closed. Thus, the donor atoms of the $XeOTeF_5^+$·SO_2ClF adduct-cation and the ion pairs presently under discussion can be viewed as approaching the xenon atoms of the parent XeF^+ and $XeOTeF_5^+$ cations at the centers of their respective tori where the positive charges of the xenon core basins are more exposed. A likely consequence of the toroidal xenon valence-electron distributions is that the xenon van der Waals radii of xenon(II) species are significantly diminished along their xenon-ligand atom bond axes (see X-ray Crystal Structure of [XeOTeF$_5$][Sb(OTeF$_5$)$_6$]·SO$_2$ClF).

The relative strengths of the donor−acceptor interactions between the xenon(II) Lewis acidic cations and the weakly fluorobasic MF_6^- (M = As, Sb) anions and SO_2ClF have been assessed on the basis of the f_{sep}-value at which the contours between the acceptor atom (xenon) and the donor atom (oxygen or fluorine) separate. Separation of the basin on the xenon atom of F_5TeOXe^+ and the oxygen atom of SO_2ClF occurs at an f_{sep} value of 0.24 and is consistent with weak, highly polar bonding and the long Xe···O(3) donor-acceptor bond (2.388 Å). The separations of the corresponding basins for XeF^+ and AsF_6^-/SbF_6^- occur at higher f_{sep} values (0.34/0.33) with no assigned bond basins, indicative of more polar-covalent bonding and in accord with long Xe···F(7) bridge bonds (2.133/2.149 Å). The separations of F_5TeOXe^+ and AsF_6^-/SbF_6^- occur at f_{sep} values (0.34/0.32) similar to those of [XeF][AsF$_6$/SbF$_6$] and have Xe···F bridge bond lengths (2.150/2.168 Å) that are also similar to those of XeF^+ salts.

The xenon valence basin (torus) volumes given by ELF population analyses decrease in the order XeF^+ (329.1) > XeF_2 (308.1) > [XeF][AsF$_6$/SbF$_6$] (272.0/268.8). For XeF^+ and XeF_2, the smaller torus volume for XeF_2 can be viewed as a contraction of the XeF^+ valence lone-pair basin volume by the negative electric field of a second fluoride ion.

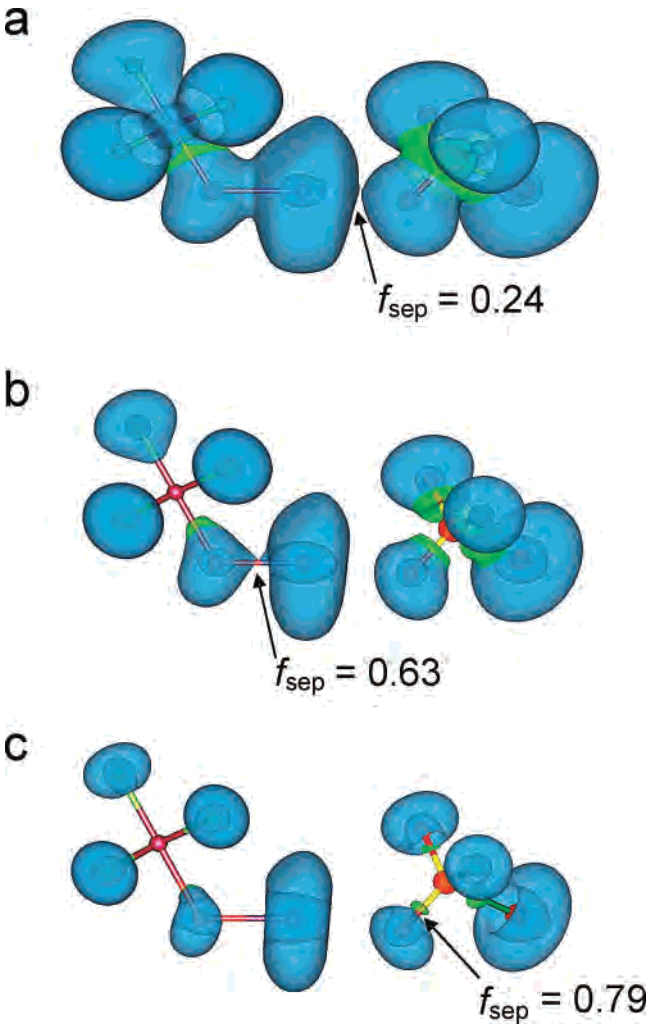

Figure 4. ELF isosurface plots at contour levels for $XeOTeF_5^+$·SO_2ClF corresponding to the indicated basin separation values, f_{sep}, at the SVWN/(SDB-)cc-pVTZ//SVWN/(SDB-)cc-pVTZ level of theory. Color scheme: blue, lone-pair (monosynaptic) basin, $V(X_i)$; green, bond (bisynaptic) basin, $V(E,X_i)$; red, core basin, C(E).

(47) Savin, A.; Nesper, R.; Wengert, S.; Fässler, T. F. *Angew. Chem., Int. Ed. Engl.* **1997**, *36*, 1808.

Although one might have anticipated the xenon lone-pair basin volume of $[XeF][AsF_6/SbF_6]$ to be intermediate with respect to those of XeF^+ and XeF_2, it is further contracted by interaction with a fluorine atom of the anion cis to the Xe···F−As/Sb bridge (Figure S2a,b). Analogous behavior is exhibited by $XeOTeF_5^+$ (307.1) and $[XeOTeF_5][AsF_6/SbF_6]$ (241.4/239.1), and moreover, the contraction is even more pronounced and might be a consequence of the higher natural charge on oxygen (O, −0.870; F: −0.327). In addition to the (F-on-M)···Xe interaction, the (F-on-Te)···Xe interaction also deforms the xenon lone-pair basin in the manner shown in Figure S2c,d. For the least strongly bound case, $[XeOTeF_5][SO_2ClF]$, the xenon torus volume (263.6) is less contracted with respect to that of $[XeOTeF_5][AsF_6]$ and is indicative of a weaker donor−acceptor interaction with SO_2ClF than with AsF_6^-/SbF_6^-. In all cases, the xenon lone-pair volumes are sensitive to nearest-neighbor interactions and correlate with the strength of the donor−acceptor interaction as assessed on the basis of their f_{sep}-values.

Conclusions

The present study provides a reliable synthesis of the strong oxidant noble-gas salt $[XeOTeF_5][Sb(OTeF_5)_6]\cdot SO_2ClF$, which is of proven and potential synthetic utility. The structural characterization of $[XeOTeF_5][Sb(OTeF_5)_6]\cdot SO_2ClF$ in solution and in the solid state has provided insight into its low-temperature oxidant properties, which are primarily consequences of the weakly coordinating nature of the $Sb(OTeF_5)_6^-$ anion, the weak Xe···O donor−acceptor bond between $XeOTeF_5^+$ and SO_2ClF, and the high solubility of the salt in SO_2ClF at low temperatures. The study has afforded a rare example of the weak Lewis base SO_2ClF coordinated to a Lewis acid center, $XeOTeF_5^+$. As well as reproducing the geometric parameters and vibrational frequencies of the $XeOTeF_5^+\cdot SO_2ClF$ adduct-cation, quantum mechanical calculations have provided consistent trends for the relative strengths of the Xe···O donor−acceptor bond in $XeOTeF_5^+\cdot SO_2ClF$ and related ion-pair bonds in $[XeL][MF_6]$ (L = F, $OTeF_5$; M = As, Sb) based on their gas-phase complexation energies and NBO and ELF analyses. These weak interactions are highly polar in nature, with $XeOTeF_5^+\cdot SO_2ClF$ providing the weakest donor−acceptor interaction within the series that was examined. The use of ELF separation contours has provided a semiquantitative approach to assessing the relative strengths of the donor−acceptor interactions in these species and might be generally applicable. The ELF calculations also show that the three valence-electron lone pairs on xenon(II) are not localized in three discreet pairs, but rather combine to form a torus around the xenon atom. Even when the coordination about the xenon atom is highly asymmetric, this toroidal electron-pair density distribution survives, albeit distorted.

Experimental Section

Apparatus and Materials. Manipulations of volatile materials were carried out on a glass vacuum line, whereas air-sensitive, involatile materials were handled inside a drybox as previously described.[15] All reaction vessels were constructed from $^1/_4$-in.-o.d. FEP tubing and joined to Kel-F valves by means of compression fittings. Reaction vessels were dried under vacuum for several hours prior to passivation with 1 atm of fluorine gas for 8−12 h. Vacuum line connections were made using $^1/_4$-in. stainless steel Cajon Ultratorr unions fitted with Viton O-rings. Oxygen-17-enriched water (^{16}O, 35.4%; ^{17}O, 21.9%; ^{18}O, 42.7%; Bureau de Rayonnements Ionisants, Saclay, France) was used without further purification. Sulfuryl chloride fluoride, SO_2ClF (Allied Chemical), was purified using the standard literature method.[48] The syntheses of $B(OTeF_5)_3$[49,50] and $Xe(OTeF_5)_2$[5] have been described elsewhere. The synthesis of $[^{17,18}O]$-$Xe(OTeF_5)_2$ from XeF_2 and $[^{17,18}O]$-$B(OTeF_5)_3$ followed the same procedures as outlined above for the precursors having natural oxygen isotope abundances. A sample of $[^{17,18}O]$-$HOTeF_5$, which was used to prepare $[^{17,18}O]$-$B(OTeF_5)_3$, was synthesized from TeF_6 and $[^{17,18}O]$-H_2O by use of a method previously outlined for the synthesis of $[^{18}O]$-$HOTeF_5$.[51]

Synthesis of $[XeOTeF_5][Sb(OTeF_5)_6]\cdot SO_2ClF$. *CAUTION! The oxidative aggressiveness of $[XeOTeF_5][Sb(OTeF_5)_6]\cdot SO_2ClF$ is manifested in the ability of the dry salt and its SO_2ClF solutions to oxidize and crack the bodies of the Kel-F valves used in the synthesis and handling of this compound should it come into contact with valve surfaces.* In a typical synthesis, 0.49654 g (0.5929 mmol) of $Sb(OTeF_5)_3$ and 0.72192 g (1.1864 mmol) of $Xe(OTeF_5)_2$ were weighed out and added to a 25-cm-long, $^1/_4$-in.-o.d. FEP reaction vessel maintained at −120 °C inside a drybox. The reaction vessel was removed cold from the drybox and immediately placed inside a −78 °C bath and connected to a glass vacuum line, where SO_2ClF solvent (ca. 3 mL) was condensed into the reaction vessel under static vacuum at −196 °C. The reactor was warmed to −20 °C, whereupon the reactants dissolved to give a colorless solution and the reaction proceeded with the liberation of xenon gas to give an intense yellow solution. The reaction vessel was periodically cooled to −78 °C and opened to the vacuum line manifold to remove xenon gas. After 3 h at −20 °C, the reactor was warmed to 0 °C for several minutes to ensure that the reaction was complete. The solvent was then removed under vacuum at −78 °C to yield a pale yellow powder and was then pumped at 0 °C for ca. 30 min to give $[XeOTeF_5][Sb(OTeF_5)_6]\cdot SO_2ClF$.

Raman Spectroscopy. (a) Raman Sample Preparation. Inside the drybox, 0.071 g (0.037 mmol) of $[XeOTeF_5][Sb(OTeF_5)_6]\cdot SO_2ClF$ at −120 °C was transferred, by use of a precooled syringe for solids, into a 25-cm-long, $^1/_4$-in.-o.d. FEP reaction vessel maintained at −120 °C. The cold reaction vessel was closed with a Kel-F valve, and the contents were then removed from the drybox; immediately placed in a −78 °C bath; and connected to a glass vacuum line, where SO_2ClF solvent (ca 1.5 mL) was condensed into the reaction vessel under static vacuum at −196 °C. The solvent was pumped under dynamic vacuum at −78 °C for several hours and periodically monitored by Raman spectroscopy to obtain different $SO_2ClF/[XeOTeF_5][Sb(OTeF_5)_6]\cdot SO_2ClF$ ratios (vide supra). When it was apparent that the adducted SO_2ClF could no longer be removed at this temperature, the sample was pumped for an additional 3 h at 0 °C to obtain a sample free of uncoordinated SO_2ClF. Raman spectroscopy indicated that the salt was stable at this temperature, and that no further SO_2ClF was removed. Because $[XeOTeF_5][Sb(OTeF_5)_6]\cdot SO_2ClF$ is unstable at room temperature,

(48) Schrobilgen, G. J.; Holloway, J. H.; Granger, P.; Brevard, C. *Inorg. Chem.* **1978**, *17*, 980.
(49) Sladky, F.; Kropshofer, H.; Leitzke, O. *J. Chem. Soc., Chem. Commun.* **1973**, 134.
(50) Kropshofer, H.; Leitzke, O.; Peringer, P.; Sladky, F. O. *Chem. Ber.* **1981**, *114*, 2644.
(51) Miller, P. K.; Abney, K. D.; Rappé, A. K.; Anderson, A.; Strauss, S. H. *Inorg. Chem.* **1988**, *27*, 2255.

the precise amount of adducted SO_2ClF could not be directly determined by mass balance.

(b) Raman Instrumentation and Spectral Acquisition. The low-temperature (−160 °C) Raman spectra of three $SO_2ClF/[XeOTeF_5][Sb(OTeF_5)_6]\cdot SO_2ClF$ samples, corresponding to molar ratios of 7.95:1.00 and 1.09:1.00 and a sample containing no uncoordinated SO_2ClF, were recorded on a Bruker RFS 100 FT Raman spectrometer using 1064-nm excitation and a resolution of 1 cm^{-1} as previously described.[52] The spectra were recorded using a laser power of 300 mW and a total of 1200 scans for each acquisition.

Nuclear Magnetic Resonance Spectroscopy. (a) NMR Sample Preparation. An NMR sample of $[XeOTeF_5][Sb(OTeF_5)_6]$ was prepared in a 5-mm-o.d. thin-wall precision glass NMR tube (Wilmad) fused to a $^1/_4$-in.-o.d. length of glass tubing that was, in turn, attached to a 4-mm J. Young Teflon stopcock by use of a $^1/_4$-in. stainless steel Cajon Ultratorr union fitted with Viton O-rings. Inside the drybox, ca. 0.1 g of $[XeOTeF_5][Sb(OTeF_5)_6]$ at −120 °C was transferred by use of a precooled syringe for solids into a dry NMR tube kept at the same temperature. The tube was then removed from the drybox; placed in a −78 °C bath; and connected to the vacuum line, where ca. 0.5 mL of SO_2ClF was statically distilled onto the sample at −196 °C. The NMR tube was then flame sealed under dynamic vacuum and stored at −196 °C until NMR spectra could be obtained.

(b) NMR Instrumentation and Spectral Acquisition. Fluorine-19, ^{125}Te, and ^{129}Xe nuclear magnetic resonance spectra were recorded unlocked (field drift < 0.1 Hz h^{-1}) on a Bruker DRX-500 spectrometer equipped with an 11.744-T cryomagnet. The ^{17}O and ^{121}Sb NMR spectra were obtained on a Bruker AM-500 spectrometer using a 10-mm broad-band VSP probe tunable over the range 23−202 MHz. For low-temperature work, the NMR probe was cooled using a nitrogen flow and variable-temperature controller (BV-T 3000).

The ^{19}F NMR spectrum was acquired using a 5-mm combination ^{1}H/^{19}F probe operating at 470.571 MHz. The spectra were recorded in a 64 K memory, with a spectral width setting of 24 kHz, yielding a data-point resolution of 0.36 Hz/data point and acquisition time of 1.39 s. A relaxation delay of 0.1 s was applied, and 3500 transients were accumulated. A line broadening of 0.1 Hz was used in the exponential multiplication of the free induction decays prior to Fourier transformation. The ^{125}Te (^{129}Xe) NMR spectra were obtained using a 5-mm broad-band inverse probe operating at 157.884 (138.871) MHz. The spectra were recorded in a 64 (32) K memory, with a spectral width setting of 63.5 (55.5) kHz, yielding a data-point resolution of 0.97 (1.69) Hz/data point and acquisition time of 0.52 (0.29) s. A relaxation delay of 0.1 s was applied, and 20 000 (100 000) transients were accumulated. Line broadening was 5 Hz in both cases. The ^{17}O (^{121}Sb) NMR spectra were obtained using a 10-mm broad-band VSP probe operating at 67.801 (59.864) MHz. The spectra were recorded in a 8 (16) K memory, with a spectral width setting of 20.0 (50.0) kHz, yielding a data-point resolution of 4.88 (6.10) Hz/data point and acquisition time of 0.20 (0.16) s. No relaxation delays was applied, and 7000 (2000) transients were accumulated. Line broadening was 5 (10) Hz. Pulse widths (μs), corresponding to a tip angle of approximately 90°, were 6.4 (^{17}O), 7.35 (^{19}F), 13.0 (^{121}Sb), 9.0 (^{125}Te), and 10.0 (^{129}Xe). The ^{17}O, ^{19}F, ^{121}Sb, ^{125}Te, and ^{129}Xe spectra were referenced externally at 30 °C to samples of neat H_2O, $CFCl_3$, 0.1 M $[N(C_2H_5)_4][SbF_6]$ in CH_3CN, $Te(CH_3)_2$, and $XeOF_4$, respectively. The chemical shift convention used is that a positive (negative) sign indicates a chemical shift to high (low) frequency of the reference compound.

X-ray Crystallography. (a) Crystal Growth of $[XeOTeF_5][Sb(OTeF_5)_6]\cdot SO_2ClF$. Inside the drybox, ca. 0.2 g of $[XeOTeF_5][Sb(OTeF_5)_6]\cdot SO_2ClF$ at −120 °C was transferred to a T-shaped $^1/_4$-in.-o.d. FEP reactor kept at the same temperature and dissolved in the minimum amount (ca 0.5 mL) of SO_2ClF. Crystals were grown by slow cooling of the reaction mixture from −50 to −80 °C over a period of 2 days inside the vertical arm of the reaction vessel. Pale yellow, block-shaped crystals were isolated by decanting the solvent into the horizontal arm, followed by drying under dynamic vacuum at −80 °C.

(b) Crystal Mounting and X-ray Data Collection. The crystal was mounted at −100 ± 3 °C as previously described[52] and centered on a P4 Siemens diffractometer, equipped with a Siemens SMART 1K CCD area detector, controlled by SMART,[53] and a rotating anode emitting Kα radiation monochromated ($\lambda = 0.710\ 73$ Å) by a graphite crystal. Diffraction data collection (−173 °C) consisted of a full ψ rotation at $\chi = 0°$ (using 1040 + 30) 0.3° frames, followed by a series of short (80 frames) ω scans at various ψ and χ settings to fill the gaps. The crystal-to-detector distance was 5.012 cm, and the data collection was carried out in a 512 × 512 pixel mode using 2 × 2 pixel binning. Raw data were processed using SAINT+,[53] which applied Lorentz and polarization corrections to three-dimensionally integrated diffraction spots. The program SADABS[54] was used for the scaling of diffraction data, the application of a decay correction, and an empirical absorption correction on the basis of the intensity ratios of redundant reflections.

(c) Solution and Refinement of the Structure. The XPREP[55] program was used to confirm the unit cell dimensions and the crystal lattice. The solution was obtained by direct methods, which located the positions of the atoms defining the $Sb(OTeF_5)_6^-$ anion, the $XeOTeF_5^+$ cation, and the SO_2ClF molecule. The final refinement was obtained by introducing anisotropic thermal parameters and the recommended weightings for all of the atoms. The maximum electron densities in the final difference Fourier map were located near the heavy atoms. All calculations were performed using the SHELXTL-plus package[55] for the structure determination and solution refinement and for the molecular graphics.

Calculations. Electronic structure calculations were carried out at the HF and SVWN (DFT) (for geometry optimizations and vibrational frequencies and intensities) levels of theory using the program Gaussian 98 (revision A.11).[56] The standard all-electron Stuttgart (2d) and cc-pVTZ basis sets as implemented in the Gaussian program were utilized for all elements except As, Te, Xe, and Sb, for which the semirelativistic large-core (RLC)

(52) Gerken, M.; Dixon, D. A.; Schrobilgen, G. J. *Inorg. Chem.* **2000**, *39*, 4244.

(53) *SMART*, release 5.054, and *SAINT*, release 6.01; Siemens Energy and Automation Inc.: Madison, WI, 1999.

(54) Sheldrick, G. M. *SADABS (Siemens Area Detector Absorption Corrections)*. University of Göttingen, Göttingen, Germany. Personal communication, 1998.

(55) *SHELXTL-plus*, release 5.1; Siemens Analytical X-ray Instruments, Inc.: Madison, WI, 1998.

(56) Frisch, M. J.; Trucks, G. W.; Schlegel, H. B.; Scuseria, G. E.; Robb, M. A.; Cheeseman, J. R.; Zakrzewski, V. G.; Montgomery, J. A., Jr.; Stratmann, R. E.; Burant, J. C.; Dapprich, S.; Millam, J. M.; Daniels, A. D.; Kudin, K. N.; Strain, M. C.; Farkas, O.; Tomasi, J.; Barone, V.; Cossi, M.; Cammi, R.; Mennucci, B.; Pomelli, C.; Adamo, C.; Clifford, S.; Ochterski, J.; Petersson, G. A.; Ayala, P. Y.; Cui, Q.; Morokuma, K.; Salvador, P.; Dannenberg, J. J.; Malick, D. K.; Rabuck, A. D.; Raghavachari, K.; Foresman, J. B.; Cioslowski, J.; Ortiz, J. V.; Baboul, A. G.; Stefanov, B. B.; Liu, G.; Liashenko, A.; Piskorz, P.; Komaromi, I.; Gomperts, R.; Martin, R. L.; Fox, D. J.; Keith, T.; Al-Laham, M. A.; Peng, C. Y.; Nanayakkara, A.; Challacombe, M.; Gill, P. M. W.; Johnson, B.; Chen, W.; Wong, M. W.; Andres, J. L.; Gonzalez, C.; Head-Gordon, M.; Replogle, E. S.; Pople, J. A.; *Gaussian 98*, revision A.11; Gaussian, Inc.: Pittsburgh, PA, 2001.

pseudopotential basis set SDB-cc-pVTZ was used.[57] The combined use of cc-pVTZ and SDB-cc-pVTZ basis sets is indicated as (SDB-)cc-pVTZ.

The program GaussView[58] was used to visualize the vibrational displacements that form the basis of the vibrational mode descriptions given in Table 5 and in the Supporting Information (Tables S1 and S2). Natural orbital analyses were performed using SVWN densities with the NBO program (versions 3.1 and 5.0).[59] The Silvi−Savin[60,61] approach to chemical bonding, which is based on a topological analysis of the gradient field of the electron localization function (ELF) of Becke and Edgecombe,[62] was conducted using the TopMod program package.[63] A complete and detailed description of the method and nomenclature can be found in ref 61, and the ELF method has also recently been summarized.[64] Slight artifactual asymmetries appear in the integrated data, which arise from the numerical grids employed in the TopMod code. Extrafine grids would remove these discrepancies, but the additional costs leading to extra precision are not expected to significantly alter the interpretations.[64] The use of pseudopotential basis set instead of an all-electron basis set was tested, and the overall results did not differ significantly, as pointed out previously.[65]

Acknowledgment. This paper is dedicated to our friend and colleague Professor Ronald J. Gillespie on the occasion of his 80th birthday and in recognition of his many outstanding contributions across a broad spectrum of chemistry. We thank the donors of the Petroleum Research Fund, administered by the American Chemical Society, for support of this work under ACS-PRF No. 40959-AC3, the Natural Sciences and Engineering Research Council (NSERC) of Canada for the award of graduate scholarships (M.D.M.) and for support in the form of a research grant (G.J.S.), the Finnish IT Center for Science for the use of their computing resources (R.J.S.), and the computational resources provided by SHARCNet (Shared Hierarchical Academic Research Computing Network; www.sharcnet.ca).

Supporting Information Available: Discussion of experimental and calculated Raman frequencies for $Sb(OTeF_5)_6^-$ and computational results for the geometries of $Sb(OTeF_5)_6^-$, XeF^+, XeF_2, [XeF][MF_6], and [$XeOTeF_5$][MF_6] (M = As, Sb). Full list of experimental and calculated geometrical parameters for $Sb(OTeF_5)_6^-$ (Table S1). Experimental Raman frequencies for [$XeOTeF_5$][$Sb(OTeF_5)_6$] in SO_2ClF (Table S2). Full list of experimental and calculated geometrical parameters and vibrational frequencies for SO_2ClF (Table S3), $XeOTeF_5^+$ (Table S4), and $XeOTeF_5^+ \cdot SO_2ClF$ (Table S5). Experimental and calculated vibrational frequencies for $Sb(OTeF_5)_6^-$ (Table S6). Calculated bond lengths, natural atomic charges, Mayer bond orders, and Mayer natural atomic orbital valencies for [XeF][MF_6], [$XeOTeF_5$][MF_6] (M = As, Sb), XeF^+, and XeF_2 (Table S7). NBO and ELF analyses for $XeOTeF_5^+ \cdot SO_2ClF$, [$XeOTeF_5$][MF_6], [XeF][MF_6] (M = As, Sb), XeF_2, and XeF^+ (Table S8) and NBO analysis for $Sb(OTeF_5)_6^-$ (Table S9). ELF isosurface plots for XeF_2, XeF^+, and $XeOTeF_5^+$ (Figure S1) and ELF isosurface plots for [XeF][MF_6] and [$XeOTeF_5$][MF_6] (M = As, Sb; Figure S2). X-ray crystallographic file in CIF format for the structure determination of [$XeOTeF_5$][$Sb(OTeF_5)_6$]$\cdot SO_2ClF$. This material is available free of charge via the Internet at http://pubs.acs.org.

IC0400890

(57) Basis sets were obtained from the Extensible Computational Chemistry Environment Basis Set Database, version 02/25/04, as developed and distributed by the Molecular Science Computing Facility, Environmental and Molecular Sciences Laboratory, Pacific Northwest Laboratory, P.O. Box 999, Richland, WA 99352.
(58) *GaussView*, release 3.0; Gaussian Inc.: Pittsburgh, PA, 2003.
(59) (a) Reed, A. E.; Weinstock, R. B.; Weinhold, F. *J. Chem. Phys.* **1985**, *83*, 735. (b) Reed, A. E.; Curtiss, L. A.; Weinhold, F. *Chem. Rev.* **1988**, *88*, 899. (c) Glendening, E. D.; Reed, A. E.; Carpenter, J. E.; Weinhold, F. *NBO Version 3.1*; Gaussian, Inc.: Pittsburgh, PA, 1990. (d) Glendening, E. D.; Badenhoop, J. K.; Reed, A. E.; Carpenter, J. E.; Bohmann, C. M.; Morales, C. M.; Weinhold, F. *NBO Version 5.0.*; Theoretical Chemistry Institute, University of Wisconsin: Madison, WI, 2001.
(60) Silvi, B.; Savin, A. *Nature* **1994**, *371*, 683.
(61) Savin, A.; Silvi, B.; Colonna, F. *Can. J. Chem.* **1996**, *74*, 1088.
(62) Becke, A. D.; Edgecombe, K. E. *J. Chem. Phys.* **1990**, *92*, 5397.
(63) Noury, S.; Krokidis, X.; Fuster, F.; Silvi, B.; *TopMod package*; Laboratoire de Chimie Théorique, University of Paris VI: Paris, 1998.
(64) Malcolm, N. O. J.; Gillespie, R. J.; Popelier, P. L. A. *J. Chem. Soc., Dalton Trans.* **2002**, 3333.
(65) Simón-Manso, Y.; Fuentealba, P. *J. Mol. Struct. (THEOCHEM)* **2003**, *634*, 89.